Preparation, Characterization, Morphological and Particle Properties of Crystallized Palm-Based Methyl Ester Sulphonates (MES) Powder

Zulina Abd Maurad [1,2,*] , **Luqman Chuah Abdullah** [2,*] , **Mohd Shamsul Anuar** [3],
Nor Nadiah Abdul Karim Shah [3] **and Zainab Idris** [1]

1 Malaysian Palm Oil Board, 6, Persiaran Institusi, Bandar Baru Bangi 43000, Selangor, Malaysia;
  zainab@mpob.gov.my
2 Department of Chemical and Environmental Engineering, Faculty of Engineering,
  Universiti Putra Malaysia, Serdang 43400, Selangor, Malaysia
3 Department of Process and Food Technology, Faculty of Engineering, Universiti Putra Malaysia,
  Serdang 43400, Selangor, Malaysia; mshamsul@upm.edu.my (M.S.A.);
  nadiahkarim@upm.edu.my (N.N.A.K.S.)
* Correspondence: zulina@mpob.gov.my (Z.A.M.); chuah@upm.edu.my (L.C.A.);
  Tel.: +603-87694339 (Z.A.M.); +603-97696288 (L.C.A.)

Abstract: Methyl ester sulphonates (MES) have been considered as an alternative green surfactant for the detergent market. Investigation on the purification of methyl ester sulphonates (MES) with various carbon chains of C_{12}, C_{14}, C_{16} and $C_{16–18}$ derived from palm methyl ester is of great interest. These MES powders have been repeatedly crystallized with ethanol and the purity of MES has increased to a maximum of 99% active content and 96% crystallinity index without changing the structure. These crystallized MES with high active content have 1.0% to 2.3% moisture content and retained its di-salt content in the range of 5%. The crystallized MES C_{16} and $C_{16–18}$ attained excellent flow characteristics. Morphology, structural and its crystallinity analyses showed that the crystals MES had good solubility properties, stable crystal structure (β polymorphic) and triclinic lateral structure when it is in high active content. The brittleness of MES crystals increased from a β′ to a β subcell. Crystal with high brittleness has the potential to ease production of powder, which leads to a reduction in the cost of production and improves efficiency.

Keywords: methyl ester sulphonates; purification; solvent crystallization; oleochemicals

1. Introduction

Methyl esters without any further modification are used as diesel substitute or biodiesel. However, due to the high content of palmitic acid and therefore higher pour point, methyl esters derived from palm oil or palm stearin are not suitable for the winter season. Palm olein needs to be used or palm methyl ester needs to be fractionated to obtain the more liquid methyl ester. With the rapid growth of the palm biodiesel where the production had increased 2.8 folds from 2016 to 2017, it will cause overcapacity of the saturated methyl ester [1]. Hence, there is a need to enhance the consumption of saturated methyl ester and one of the alternatives is to channel the saturated methyl ester as starting materials to produce methyl ester sulphonates (MES).

The technology to produce MES is available worldwide; however, there are only a few producers of this surfactant in the world, such as Malaysian Palm Oil Board (MPOB), Chemithon Corporation (United States), Lion Corporation (Japan), KLK Oleomas (Malaysia), Stephan Company (United States), Wilmar International Ltd. (Indonesia), Guangzhou Keylink Chemical Co., Ltd. (China), Guangzhou Lonkey

Industrial Co Ltd. (China) and Sinopec Jinling Petrochemical Co., Ltd. (China) [2,3]. The technology to produce palm-based MES involves sulphonation of a palm oil-based methyl ester with sulfur trioxide/air followed by digestion, bleaching and neutralizing to produce MES C_{12} and C_{14} and additional steps through the turbo tube drying and flaking system process to produce dry MES C_{16} and C_{16-18}, as summarized in Figure 1 [4].
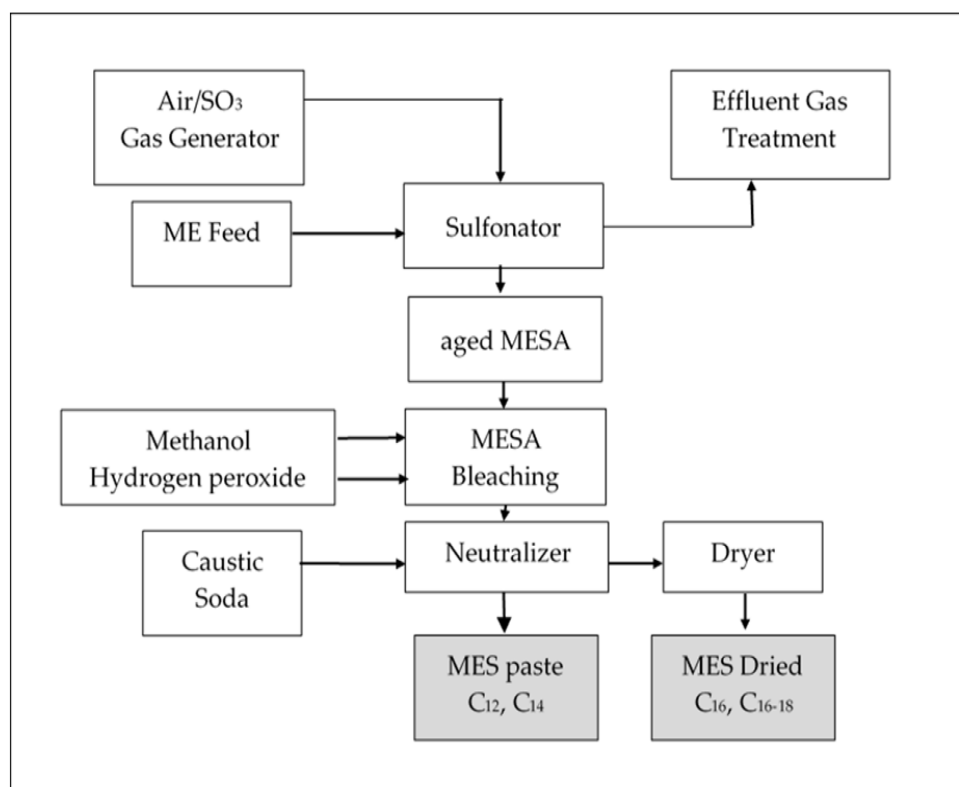

Figure 1. Block diagram for the methyl ester sulphonates (MES) process pilot plant at the Malaysian Palm Oil Board (MPOB).

The mechanism for the formation of MES has been thoroughly studied and is believed to occur through several stages of the process, as in Figure 2 [5–7]. The first stage is when sulfur trioxide is reacted with saturated fatty methyl ester and rapidly produces mono-adduct (I). The mono-adduct attaches into an intermediate that activates the carbon at the position alpha to the carboxylic group; it will then be sulphonated with a second molecule of sulfur trioxide. Then, the di-adduct rearranges to form a dark color fatty methyl ester sulfonic acid (MESA) and release of one molecule of sulfur trioxide (II). The re-arrangement of the di-adduct is a limiting step and the process continues until all esters have been sulphonated (III). In the presence of an alkali, the fatty methyl ester sulfonic acid will form MES (V), but the di-adduct will hydrolyze into a di-salt (VI).

Research results have confirmed the superior properties of palm-based MES in terms of its detergency, biodegradation [8], synergy with soap [9] and tolerance to different water hardness in comparison to LAS. Furthermore, the cost of production of MES is comparatively lower than LAS [10]. These extensive research activities and testing have confirmed that MES and its cleaning products are environmental friendly [11]. The MES and formulated palm-based cleaning products are easily biodegraded [12].
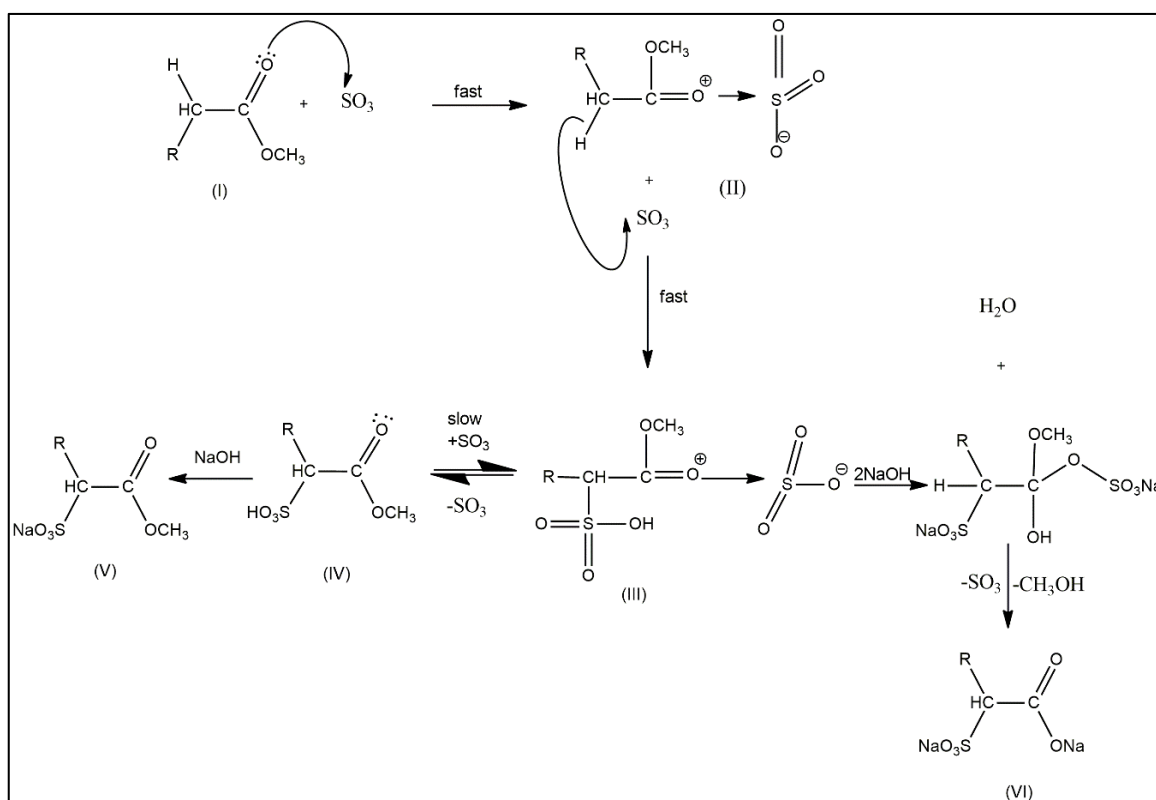
Figure 2. Reaction of methyl ester sulphonates (V) and the intermediates, such as di-salt (VI).

A major application of MES was for the detergent segment; however, Grand View Research reported that the personal care segment was anticipated to emerge for over 34% of the MES market volume share by 2025 [13]. Application flexibility is largely based on the quality of the MES; in particular, the composition and physical form of the product. In Malaysia, MES C_{16} and C_{16-18} are currently commercially available in the market under the brand name of Mizulan and Palmfonate, with an active content of ~86% and generally used in detergents. MES C_{12} and C_{14} based on palm oil are not commercially available; however, MPOB has the capability to produce the middle cut with active contents of 68% and 83%, respectively, but contained a substantial amount of water, methanol, di-salt and other impurities. These impurities in MES C_{12} and C_{14} are irritants to the eye according to the *SkinEthicTM HCE* model [14]. Successful usage of MES as an active ingredient in personal care could be achieved if the MES C_{12} and C_{14} produced were non-irritant. The objective of this preliminary study was to investigate the feasibility of employing the crystallization process with ethanol as the solvent, to produce crystallized MES powder of various carbons with 97% to 99% active content and analyzing their properties for knowledge.

2. Results and Discussion

2.1. Crystallized MES Powder

Crystallized MES powder of various carbon chain lengths (C_{12}, C_{14}, C_{16} and C_{16-18}) with 97% to 99% active content had been obtained through grinding, crystallization and drying processes. These processes were to eliminate moisture content and increase active content but retain the di-salt content. Four solvents, such as methanol, ethanol, isopropyl alcohol (IPA) and hexane, were selected to determine the solubility of MES, as in Figure 3. Ethanol was the second-highest solubility polar solvent having 6.3-2.5 mg/mL solubility with MES. MES C_{12} has the highest solvent solubility rates compared to other carbon chain lengths. The shorter the carbon chain of MES, the higher the solvent solubility rate. If the carbon chain of MES is large, the critical micelle concentration (CMC) and

solubility should decrease [15,16]. Methanol shall not be used as solvent in the purification of MES as it can increase di-salt content (undesirable) and is extremely toxic [17]. Ethanol is the most suitable solvent for the crystallization process of MES. In addition, ethanol can be made from a renewable energy fuel from sugar crops, starches or cellulosic biomass [18]. In this study, MES was not dissolved in hexane. The overall cost-benefit using co-solvent (ethanol and water) with low toxicity solvent in repeated crystallization of MES is high. The solvent crystallization process can increase product stability, which can have a positive influence in reducing manufacturing costs. However, the cost of disposal of the used solvent must be taken into consideration.
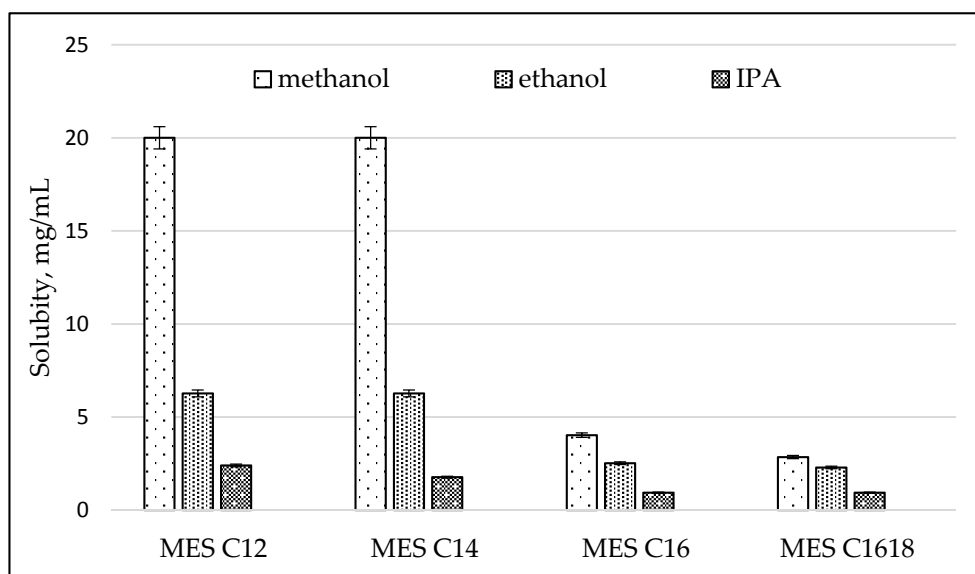

Figure 3. Solubility of MES in solvents.

The dried crystallized MES powder produced from repeated crystallization from ethanol has an active content of MES C_{12}: 98.96%, MES C_{14}: 97.76%, MES C_{16}: 99.32% and MES C_{16-18}: 99.18%. The active content of MES C_{14}, C_{16} and C_{16-18} has an increment of 15% to 19% while MES C_{12} has the highest active increment of 45%. Moisture content of MES has been dried to 1.0% to 2.3%, while di-salt content was retained less than 5%, which is desirable. A higher di-salt content leads to a lower surface activity of MES and lower hardness, as di-salt's Krafft point is higher than that of MES [19]. Crystallization can also be seen as a technique to obtain solid products, as MES C_{12} and C_{14} after repeated crystallization becomes solid powder from a paste. Other specifications of MES are shown in Table 1.

Table 1. Specifications of high active content crystallized MES powder.

Product/Parameter	MES C_{12}	MES C_{14}	MES C_{16}	MES C_{16-18}
Molecular weight	316.47	344.07	372.46	382.71
Active (%)	98.96 ± 0.04	97.76 ± 0.02	99.32 ± 0.04	99.18 ± 0.06
Di-salt/active (%)	0.42 ± 0.03	4.46 ± 0.03	4.76 ± 0.04	4.72 ± 0.01
5% Klett	11.95 ± 0.23	2.03 ± 0.45	18.08 ± 0.12	25.20 ± 0.34
pH (10%)	5.42 ± 0.02	3.89 ± 0.04	5.26 ± 0.01	5.44 ± 0.01
Moisture (%)	2.32 ± 0.12	1.03 ± 0.43	1.74 ± 0.31	2.20 ± 0.09
Appearance	——————————Powder crystals——————————			

2.2. Structural Conformation of Crystallized MES Powder

The infrared spectrum of MES before and after repeated crystallization are illustrated in Figure 4; Figure 5, respectively. Both infrareds have the same band pattern except for MES after repeated

crystallization, which has lower intensity at 3611–3420 cm^{-1} (-OH stretching) and 1640–1600 cm^{-1} (H–O–H bending region) compared to infrared from MES before crystallization. This is due to lower moisture content in high active content MES after repeated crystallization and is in agreement with the study conducted by Hongping et al. [20]. The typical peaks of the methyl group (C–H) at 2958–2849 cm^{-1} and carbonyl group (C=O) at 1724–1716 cm^{-1} were observed in both infrared. The presence of the sulfonate group (S=O) stretching vibration at the strong peak 1222–1051 cm^{-1} and (S–O) stretching at peak 857–719 cm^{-1} indicates that both compounds are methyl ester sulfonate [21,22]. The crystallization does not affect the structure of MES, but instead increased the active content and reduced the moisture content.
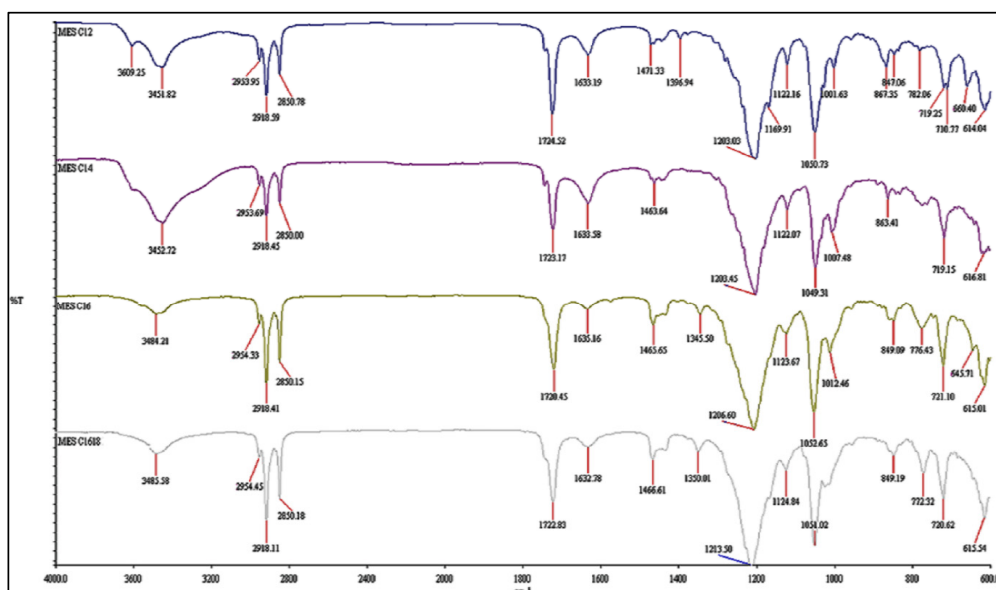

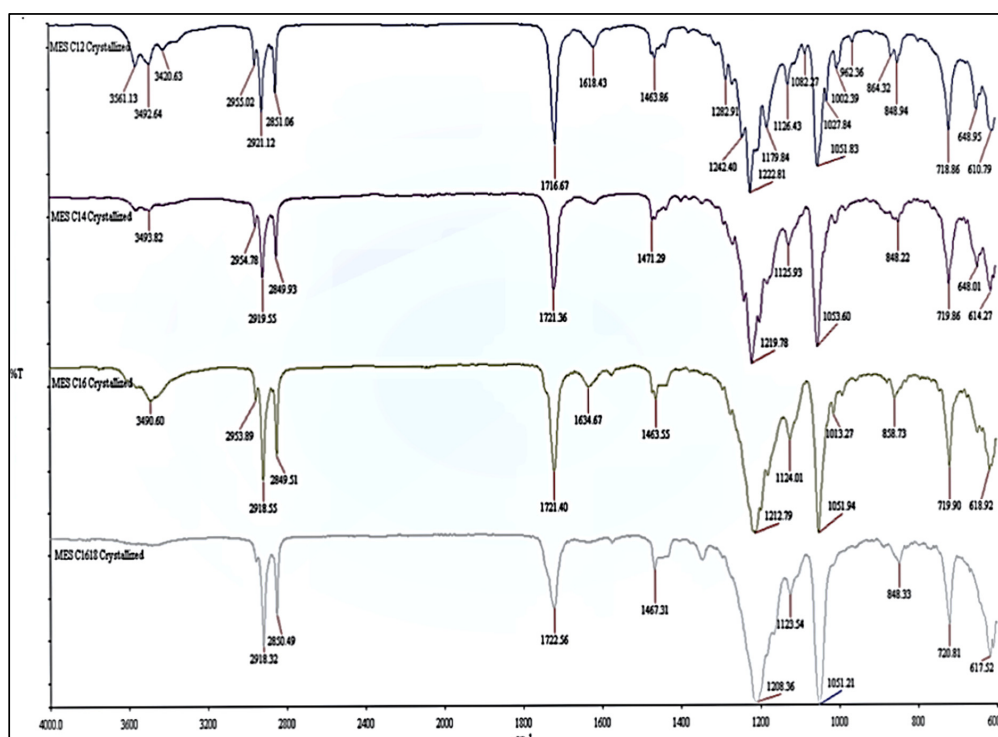**Figure 4.** Infrared of MES before crystallization.

Figure 5. Infrared of MES after repeated crystallization.

The composition of MES before and after repeated crystallization was similar and confirmed by ^{1}H and ^{13}C NMR analysis (Tables 2 and 3). The MES was dissolved in deuterium water (D_2O) and processed at 60 °C. A proton attached to the carbon atom (–CH–), which, bearing the sulfonate group, appears at peak 3.87–3.89 ppm (s, H). The peak for the hydrogen attaching to the carbon atom bearing an ester group (–COO) appears at 3.71–3.75 ppm (t, 3H). The hydrocarbon chain is observed at the peak between 0.76 and 0.80 ppm (terminal CH_3–) and 1.90 to 2.00 ppm (CH_2– linked with –CH). The difference between various MES chain lengths is at peak 1.16 to 1.21 ppm (CH_2) $_n$- with MES C_{12} (d, 16H), MES C_{14} (d, 20H), MES C_{16} (d, 24H) and MES C_{16-18} (d, 28H).

The ^{13}C-NMR spectra for all MES before and after repeated crystallization indicated that the carbon for the terminal methyl (CH_3) appears at peak 13.86 to 13.95 ppm. The carbon directly attached to the sulfonate group (–SO_3Na–CH–) is observed at peak 66.02 to 66.20 ppm. The signal for carbon directly attached to the ester group (–OCH_3–) is observed at peak 52.96 to 53.06 ppm and the carbon (C=O) appears at peak 170.52 to 170.59 ppm. Both FTIR and NMR results are in good agreement with the results obtained from the literature and prove that all are MES products [23].

Table 2. NMR spectra data of MES before and after repeated crystallization.

MES	Acyl Chain Length	Terminal CH_3–	–(CH_2) $_n$–	CH_2– Linked with –CH–	–OCH_3	S–CH–
				Assignment (δ ppm)		
				Before Crystallization		
C_{12}	12	0.74–0.76 (t, 3H)	1.17 (d, 16H)	1.92–1.97 (d, 2H)	3.71 (t, 3H)	3.87 (s, H)
C_{14}	14	0.73–0.76 (t, 3H)	1.16 (d, 16H)	1.90–1.95 (d, 2H)	3.71 (t, 3H)	3.87 (s, H)
C_{16}	16	0.73–0.76 (t, 3H)	1.17 (d, 16H)	1.91–1.96 (d, 2H)	3.71 (t, 3H)	3.87 (s, H)
C_{16-18}	16–18	0.73–0.77 (t, 3H)	1.18 (d, 16H)	1.92–1.97 (d, 2H)	3.71 (t, 3H)	3.87 (s, H)
				After Repeated Crystallization		
C_{12}	12	0.78–0.80 (t, 3H)	1.21 (d, 16H)	2.00 (d, 2H)	3.75 (t, 3H)	3.89 (s, H)
C_{14}	14	0.74–0.76 (t, 3H)	1.17 (d, 16H)	1.95 (d, 2H)	3.74 (t, 3H)	3.89 (s, H)
C_{16}	16	0.74–0.76 (t, 3H)	1.17 (d, 16H)	1.99 (d, 2H)	3.73 (t, 3H)	3.89 (s, H)
C_{16-18}	16–18	0.74–0.76 (t, 3H)	1.17 (d, 16H)	2.00 (d, 2H)	3.74 (t, 3H)	3.89 (s, H)

Table 3. Nuclear magnetic resonance analysis (NMR) spectra data of MES before and after repeated crystallization.

MES	Terminal CH_3–	Adjacent (CH_2)–	(CH_2)$_n$–	–OCH_3	–CH–	C=O
			Assignment (δ ppm)			
			Before Crystallization			
C_{12}	13.86	22.68	27.39–32.06	53.04	66.09	170.54
C_{14}	13.86	22.71	27.43–32.10	53.00	66.20	170.52
C_{16}	13.93	22.74	27.47–32.13	52.97	66.04	170.52
C_{16-18}	13.93	22.72	27.49–32.16	52.96	66.02	170.52
			After Repeated Crystallization			
C_{12}	13.88	22.71	27.43–32.09	53.06	66.14	170.59
C_{14}	13.89	22.74	27.48–32.13	53.03	66.12	170.58
C_{16}	13.89	22.76	27.52–32.15	52.99	66.07	170.57
C_{16-18}	13.95	22.79	27.56–32.17	52.98	66.06	170.56

2.3. Properties of Crystallized MES Powder

2.3.1. Surface Morphology

The surface morphology of the MES before and after repeated crystallization was examined by scanning electron microscopy analysis (SEM), as shown in Figure 6. Both MES before and after repeated crystallization have an elongated spherical particle structure in clusters or in an agglomerated form, which is in agreement with a study conducted by Babu et al. [24]. Also, the particles have irregular shapes and sizes. The elemental analysis values found from energy dispersive x-ray spectroscopy (EDX) had confirmed the oxygen, sodium and sulfur contents in the MES, and values are tabulated in Table 4. No other peak for any other element can be found in the spectrums, which supports that the surfactant is MES. The surface morphology of MES C_{12} cannot be compared from before and after repeated crystallization as, initially, MES C_{12} is in paste form.

2.3.2. Particle Size (Dynamic Light Scattering)

Table 5 shows that the median diameter of particle MES increased after crystallization. With the increase in MES surfactant active content, the particle size increases simultaneously [25]. The increase of mean size diameter results from the aggregation of the molecules. Intergrowth of aggregates formed by particle collisions, through a crystallization process that forms an agglomerative bond [26].
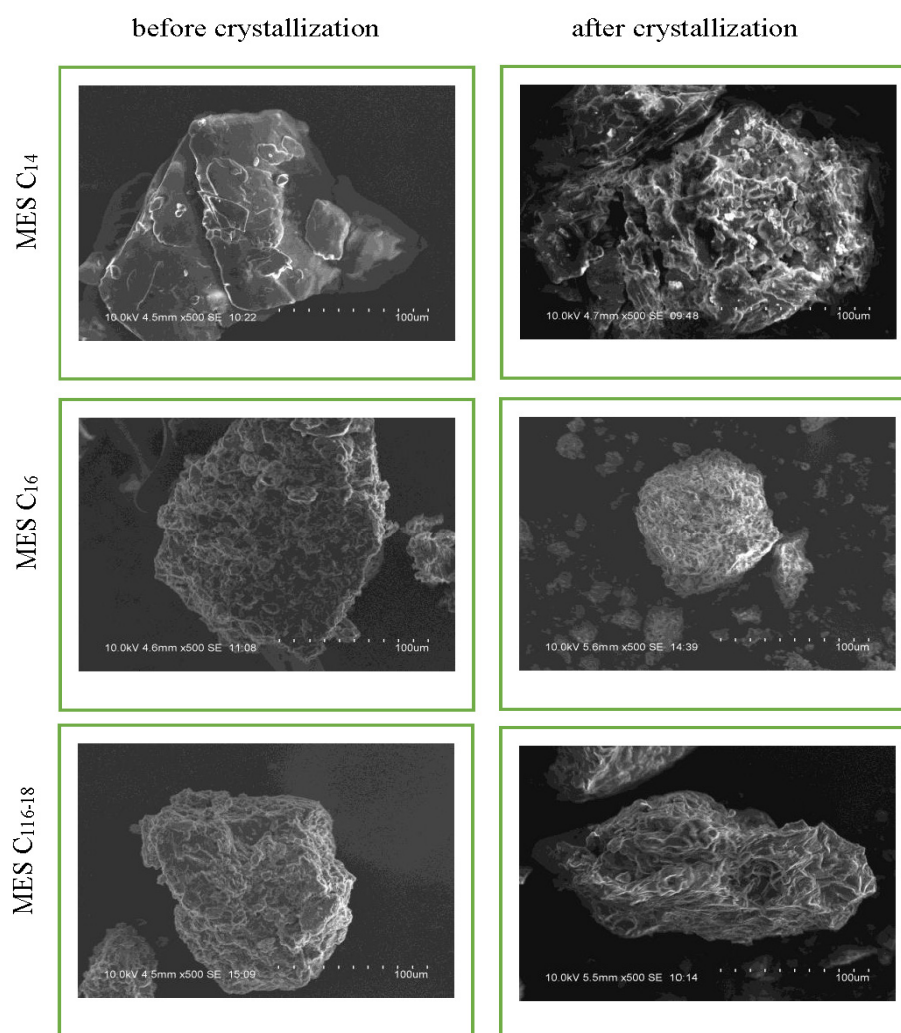

Figure 6. Surface morphology of the MES before and after repeated crystallization.

Table 4. Elemental analyses of MES.

| MES | Elemental Analyses, % | | | | | |
| | Before Crystallization | | | After Crystallization | | |
	O	Na	S	O	Na	S
C_{14}	16.44 ± 4.83	11.95 ± 2.67	14.64 ± 0.16	18.76 ± 4.89	15.22 ± 4.75	17.05 ± 1.65
C_{16}	16.72 ± 3.99	12.15 ± 1.82	15.69 ± 1.32	13.97 ± 13.62	12.18 ± 10.92	17.23 ± 1.12
C_{16-18}	19.20 ± 5.76	13.62 ± 3.70	14.65 ± 0.43	10.98 ± 8.13	8.84 ± 4.97	13.50 ± 0.87

Table 5. Particle size of MES surfactant.

| Parameter | Mean Size Diameter (µm) | | | |
	MES C_{12}	MES C_{14}	MES C_{16}	MES C_{16-18}
MES before crystallization	liquid	72.59 ± 0.44	9.99 ± 0.25	404.87 ± 1.16
MES after crystallization	5.45 ± 1.11	73.74 ± 0.11	12.52 ± 0.35	447.18 ± 1.25

2.3.3. Flow Behavior

The bulk and tapped density of palm stearin-based MES (C_{16} and C_{16-18}) before and after repeated recrystallization were evaluated in order to determine the flowability of the powder through the Carr Compressibility Index (CI) and Hausner Ratio (HR) (Figure 7). Powder MES of C_{16} and C_{16-18} before crystallization had fair and good flow characteristics, respectively, due to the existence of larger interparticle interactions; thus, a greater difference between bulk and tapped densities is observed. The HR is also affected by normal and tangential not-roundness. As the not-roundness of the cross-sectional shape increases, so too does the HR increase [27]. After repeated recrystallization, MES of C_{16} and C_{16-18} with high active content attained excellent flow characteristics. Therefore, interparticle interactions are generally less significant, for which the bulk and tapped densities have been relatively close in magnitude. In addition, the particles of MES after repeated crystallization is in pure homogeneity form.
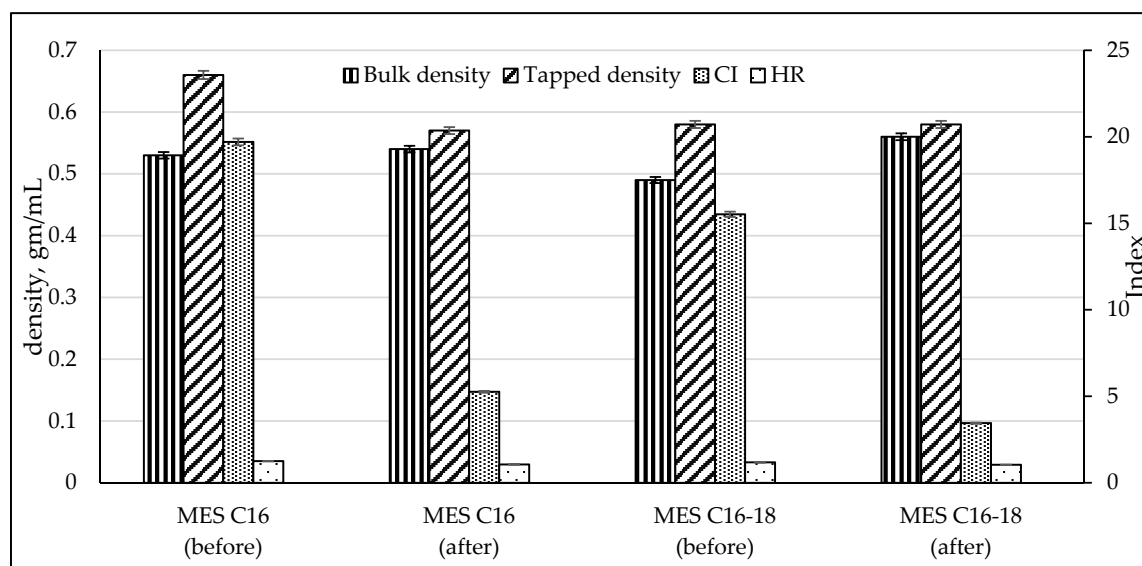

Figure 7. The bulk and tapped density of palm stearin-based MES (C_{16} and C_{16-18}) before and after repeated recrystallization.

2.3.4. Crystallinity

The detail about the crystal of MES has been evaluated using x-ray diffraction (XRD). The histograms in Figure 8 show the small angle scattering (SAXS) at $1° < 2\theta < 12°$ and wide-angle

x-ray scattering (WAXS) at 12° < 2θ < 35° of MES C_{12}, C_{14}, C_{16} and C_{16-18} before (low active content) and after repeated crystallization (high active content). The SAXS pattern of MES gives information about the lamellae and crystal thickness while WAXS gives information on polymorphism of the MES.

A study by Larsson [28] states that the primary forms of polymorphic are α, β′ and β. From the histograms, the MES C_{12}, C_{14}, C_{16} and C_{16-18} after repeated crystallization (high active content) and MES C_{16-18} before crystallization has a β polymorphic form, which is the most stable arrangement and will result in a coarse and grainy texture [29]. This is due to the peak that appears at positions d = 4.6, 3.8 and 3.7 Å. The Bragg peaks define these subcells within the crystal lattice of a triclinic [30]. The MES C_{12} and C_{14}, before (low active content), do not have any peak position for α, β′ and β but MES C_{16} has peaks appearing at positions d = 4.2 and 3.8 Å, which confirms the β′ polymorphic (orthorhombic crystal lattice) form according to the XRD AOCS method [31].

The crystalline structure of MES was transformed from metastable crystal (α subcell) to a mixture of anhydrous crystals (β subcell) and dihydrate crystals (β′ subcell) owing to melt-mediated crystallization. The brittleness of MES crystals increased from an α to a β′ to a β subcell. Transformation into more brittle crystals will lead to a decreased yield value of MES [32]. Crystals with low brittleness are disadvantageous during manufacturing processes because enormous amounts of energy are required to convert them into powder.
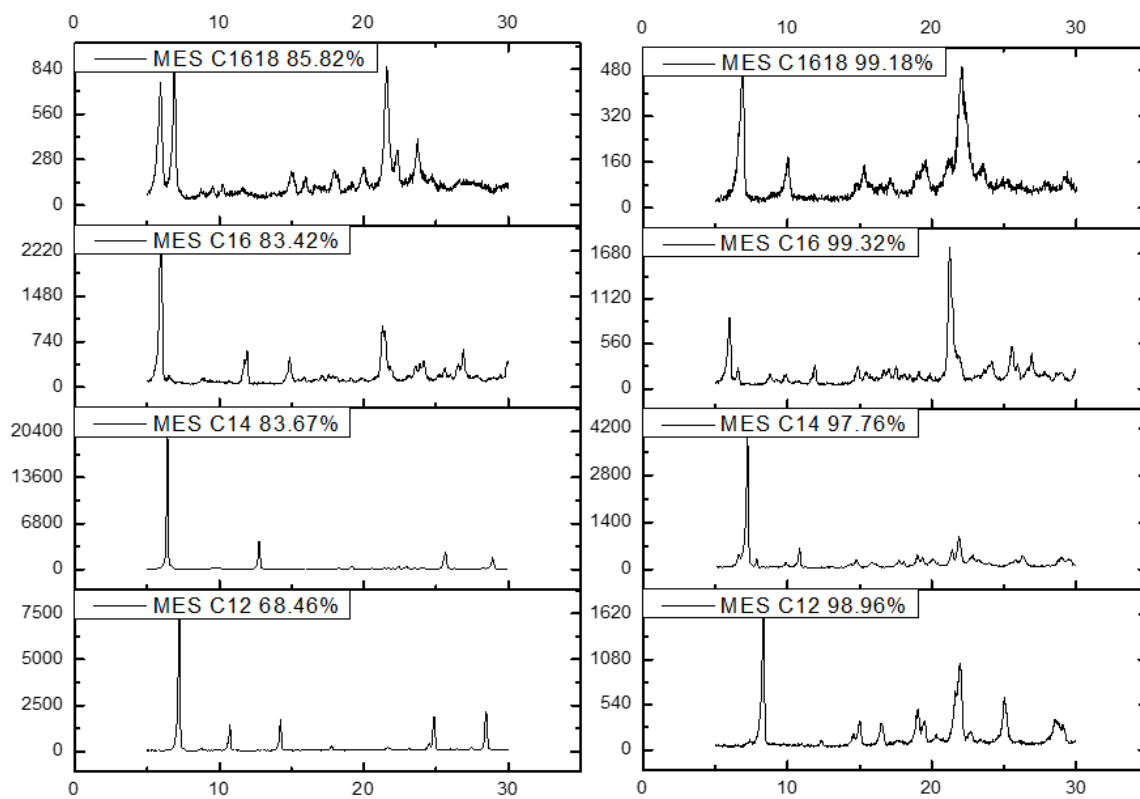

Figure 8. X-ray diffraction (XRD)-histograms of MES C_{12}, C_{14}, C_{16} and C_{16-18} before (left) and after crystallization (right).

The crystallized MES (C_{12}, C_{14}, C_{16} and C_{16-18}) has a crystallinity index more than 96% (Figure 9) based on the Segal equation, as stated in the equation [33]: Crystallinity Index, CrI (%) $= \frac{I_{002} - I_{am}}{I_{002}} X 100$. The Segal method is based on two parts of crystalline and amorphous. The amount of crystalline material is implied by the height of the highest diffraction peak (I_{002}), and the amount of amorphous material is implied by the height of the minimum intensity between the major peaks (I_{am}). The CI is the difference between these two intensities, divided by the intensity of the highest peak (I_{002}).
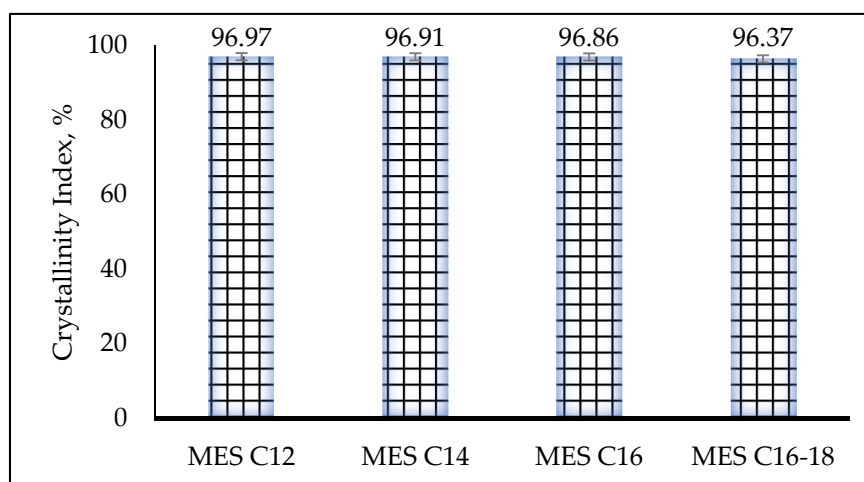
Figure 9. Crystallinity Index (CrI) of MES after repeated crystallization.

2.3.5. Solubility

Good water solubility properties at ambient temperature make the product easy to incorporate in liquid formulations. The solubility of MES before crystallization and after repeated crystallization has been determined (Figure 10). The higher the purity of MES (C_{14}, C_{16} and $C_{16–18}$), the better the solubility except for MES C_{12} because impurities generally lead to reduced CMCs, thus reduce the solubility [34]. MES C_{12} before crystallization is already in liquid form and has a hydrogen bond and is, therefore, easier to dissolve. The pure MES C_{14} has higher solubility compared to MES C_{16} and MES $C_{16–18}$. The solubility decreases with an increase in molecular weight [35].
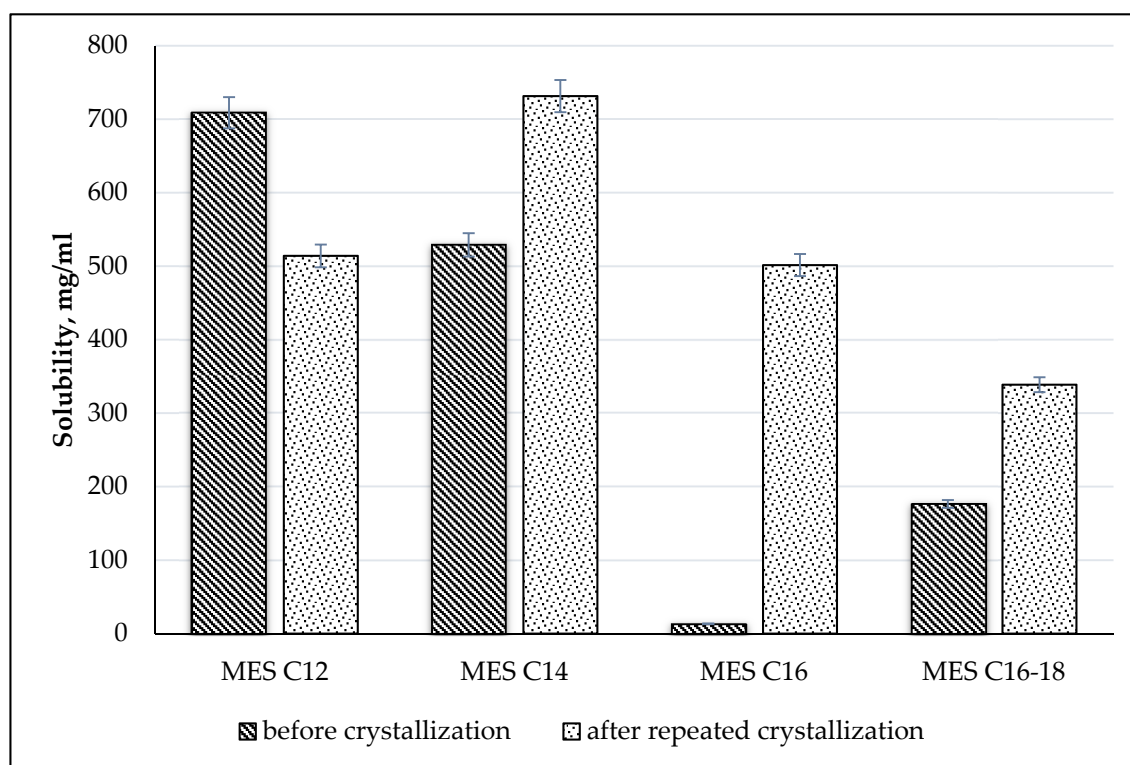

Figure 10. Solubility of MES with different active content in water.

2.3.6. Melting Point

A melting point is a useful indicator of purity as there is a general lowering and broadening of the melting range as impurities increase. Table 6 indicates the melting point of MES with different purities according to active content. The higher the active content of MES of each chain length, the greater the melting point increase; thus, the impurities have been eliminated. The melting point of alkyl α-sulfopalmitates (C_{14}) and stearates (C_{16}) has been reported by Weil et al. with values of 180.9–182.8 and 179.8–180.0 °C, respectively, but their preparation in a state of purity has not been adequately described [36].

Table 6. Melting point of MES.

Parameter	Melting Point Capillary Tube, °C			
	MES C_{12}	MES C_{14}	MES C_{16}	MES $C_{16–18}$
Before crystallization	131.0 ± 0.4	116.3 ± 0.2	186.5 ± 0.1	209.2 ± 0.3
After repeated crystallization	203.1 ± 0.2	217.8 ± 0.4	197.8 ± 0.0	229.5 ± 0.4

3. Materials and Methods

3.1. Materials

MES produced from MPOB usually has an active content of 83% to 86% for MES C_{14}, C_{16} and $C_{16–18}$ and 68% for lower chain MES C_{12}. It has very low color (<25 Klett color) and low di-salt content, (<5%). Other specifications as listed in Table 7.

Table 7. Technical specifications of MES with different carbon chain lengths produced from MPOB's MES plant.

Product/Parameter	MES C_{12}	MES C_{14}	MES C_{16}	MES $C_{16–18}$
Molecular weight	316.47	344.07	372.46	382.71
Active (%)	68.46 ± 0.07	83.67 ± 0.05	83.42 ± 0.06	85.82 ± 0.09
Di-salt/active (%)	1.03 ± 0.05	4.18 ± 0.07	4.30 ± 0.10	4.02 ± 0.07
5% Klett colour	7.14 ± 0.11	20.23 ± 0.15	21.89 ± 0.09	24.11 ± 0.12
pH (10%)	4.88 ± 0.03	3.29 ± 0.02	5.38 ± 0.03	5.52 ± 0.02
Moisture (%)	21.95 ± 0.24	14.03 ± 0.25	9.20 ± 0.19	8.92 ± 0.22
Appearance	semi-liquid	paste	flakes	flakes

3.2. Preparation of Crystallized MES Powder

MES of various carbon chain lengths (C_{12}, C_{14}, C_{16} and $C_{16–18}$) were highly purified by repeated recrystallization from ethanol. MES C_{12} and C_{14} were in semi-liquid and paste forms, respectively. While MES C_{16} and $C_{16–18}$ that are in flake form will need to be grounded until a particle size of at least of 700 to 750 μm is achieved using a high shear knife mixer. No preheating was needed to prevent the sample from evaporating. MES was then mixed with hot ethanol/ distilled water mixtures (95/5 by volume) and stirred using a magnetic bar with 1000 to 1050 rpm for 20 to 60 min depending on the physical form of MES and the solubility properties. The total amount of solvent used with the MES to solvent ratio (wt/wt%) were 1:1, 1:2 and 1:3 depending on the concentration of the mixture. The mixture of MES and solvent were left to cool down and crystallize in a glass refrigerator with a temperature of 4.5 to 5 °C without any mechanical induced convective airflow. The crystallization time was set to 24 h. After 24 h of crystallization, the crystals were emptied onto a bush funnel and filter paper with a 6 μm pore size and connected to a jet water aspirator to perform vacuum filtration. The filtration process to segregate the MES crystals from the mother liquor took 240 min. The semi-dry crystal particles MES were recrystallized again for another two or three cycles to obtain highly purified MES. After the repeated recrystallization, the semi-dry crystal particles MES were scattered on plastic trays and subjected to mechanically induced ventilation for 24 h. This drying process was carried out

under normal room temperature at 27 °C. The dried MES crystal particles were then stored in the presence of silica gel as a drying agent. The yield of repeated crystallization for MES C_{14}, C_{16} and C_{16-18} was 96% and a lower yield for MES C_{12} with 85%. All experiments and analyses were conducted in duplicates in order to ensure reproducibility.

3.3. Analyses

3.3.1. MES Specifications

The method for specifications of MES was described by Battaglini et al. [37]. The di-salt content was determined from two titrations (methylene blue and phenol red titration) and a result from the free oil determination. The measurement for color was determined by Klett–Summerson colorimeter (Bel-Art Products, Scienceware, USA). All analyses were performed in duplicate with data reported representing average values.

3.3.2. Active Content

The active component or purity of the surfactant in detergent was determined by titration procedure (anionic) according to The Chemithon Analytical Method 1101.2 [38] based on ASTM D3049 [39]. The analysis was performed in triplicate with data reported representing average values.

3.3.3. Moisture Content

The moisture content of MES was determined using the Mettler Toledo, C30 Karl Fischer Compact Titrator (Switzerland) and the method specified by Scholz [40] according to AOCS Ca 2e-84.

3.3.4. Fourier Transform—Infrared Analysis

The Fourier Transform—Infrared spectroscopy (FTIR) analysis was carried out to determine the functional group(s) present in the MES compound according to Nikolic [41]. This Spectrum 100 equipped with attenuated total reflectance unit was from Perkin Elmer (USA). The spectral range in wave-numbers for the spectrophotometer was set at 4000 to 600 cm^{-1}, and the final output presentation was in percent transmittance.

3.3.5. Nuclear Magnetic Resonance Analysis (NMR)

The structure of MES was identified by ^{1}H and ^{13}C NMR analyses with deuterium water as the solvent using a JOEL RESONANCE, model EC2 600R, 600 MHz (Japan).

3.3.6. Scanning Electron Microscopy Analysis

The Scanning Electron Microscopy (SEM) analysis was carried out to observe the morphology of the MES crystals formed using Hitachi S-3400N (Japan) coupled with energy dispersive x-ray spectroscopy (EDX), model Bruker X Flash 6I10 (US). The Quantax System, ESPRIT software was used for data acquisition and analysis.

3.3.7. Particle Size Distribution Analysis

The Particle Size Distribution (PSD) of powder MES was measured in ethanol by using Malvern Instruments Mastersizer 2000 and the Hydro 2000S particle size analyzer (United Kingdom) at room temperature, 27 °C. Each sample was repeated in duplicate to ensure good repeatability. The PSD was characterized by the median diameter.

3.3.8. Flow behavior

The Carr Compressibility Index (CI) and Hausner Ratio (HR) are two measures that can be used to predict the propensity of a given powder sample to be compressed, and which are understood to reflect the importance of interparticle interactions. The CI and HI are calculated using the following relations:

$$\text{Carr Compressibility Index (CI)} = \frac{\text{tapped density} - \text{bulk density}}{\text{tapped density}} \times 100 \qquad (1)$$

$$\text{Hausner Ratio (HR)} = \frac{\text{tapped density}}{\text{bulk density}} \qquad (2)$$

A CI of <10 or HR of <1.11 is considered 'excellent' flow whereas CI > 38 or HR > 1.60 is considered 'very very poor' flow. There are intermediate scales for CI between 11 and 15 or HR between 1.12 and 1.18 is considered 'good' flow, CI between 16 and 20 or HR between 1.19 and 1.25 is considered 'fair' flow, CI between 21 and 25 or HR between 1.26 and 1.34 is considered passable flow, CI between 26 and 31 or HR between 1.35 and 1.45 is considered 'poor' flow, and CI between 32 and 37 or HR between 1.46 and 1.59 is considered 'very poor' flow [42,43].

3.3.9. X-ray Diffraction

The powder X-ray diffraction (XRD) measurement was carried out using XRD 6000 Shimadzu (Japan) equipped with basic process software for data acquisition and analysis. About a 200–500 mg sample was ground and mounted on an alumina sample holder. Data were acquired using a Cu monochromatized radiation source operated at 30 kV and 30 mA. The intensity data were recorded by a continuous scan in the diffraction angle 2θ from $5°$ to $30°$ with a step size of $0.02°$.

3.3.10. Melting Point

The melting point of MES was determined according to a capillary tube method using Electrothermal 9100 (Essex, UK).

4. Conclusions

Purification of MES powder has been conducted through a crystallization process with ethanol as the solvent. The process successfully achieved more than 97% active content instead of 86%, 1.0% to 2.3% moisture content and retained its di-salt content in the range of 5%. Through crystallization also, MES C_{12} and C_{14} were converted to solid powder. The composition of MES before and after repeated crystallization were similar and confirmed by infrared spectrum, ^{1}H and ^{13}C NMR analysis. Crystallized MES powder has an elongated spherical particle structure in clusters or in an agglomerated form. With the increase in MES surfactant active content, the particle size increases simultaneously. Crystallized MES C_{16} and C_{16-18} with high active content attained excellent flow characteristics. Crystallized MES C_{12}, C_{14}, C_{16} and C_{16-18} with high active content have a β polymorphic form and triclinic lateral structure, which is the most stable arrangement, and have a crystallinity index more than 96%. The brittleness of MES crystals increased when at the β subcell form. Therefore, the production of powder will require high brittleness of MES to reduce the cost. The higher the purity of MES, the better the solubility. The solubility decreases with an increase in molecular weight. The crystallized MES C_{12}, C_{14}, C_{16} and C_{16-18} with high active content have melting points of 203, 217, 197 and 229 °C, respectively. The crystallization of MES is a great process to produce high active MES for product specification.

5. Patents

There is patent filed number PI2019005429, resulting from the work reported in this manuscript.

Conflicts of Interest: The authors declare no conflict of interest.

References

1. Kushairi, A.; Loh, S.K.; Azman, I.; Hishamuddin, E.; Ong-Abdullah, M.; Izuddin, Z. Oil palm economic performance in Malaysia and R&D progress in 2017. *J. Oil Palm Res.* **2018**, *30*, 163–195.

2. Maurad, Z.A.; Idris, Z.; Ghazali, R. Performance of Palm-Based C16/18 Methyl Ester Sulphonate (MES) in Liquid Detergent Formulation. *J. OLEO Sci.* **2017**, *66*, 677–687. [CrossRef]

3. Market, A. Global Industry Analysis, Size, Share, Growth, Trends and Forecast 2016–2024. 2018. Available online: https://www.transparencymarketresearch.com/logistics-market.html (accessed on 20 February 2020).

4. Foster, N.C.; MacArthur, B.W.; Sheats, W.B.; Shea, M.C.; Trivedi, S.N. *Production of Methyl Ester Sulfonates. Handbook of Detergents, Part F: Production*; CRC Press: Boca Raton, FL, USA, 2008; Volume 142, p. 201.

5. Kapur, B.; Solomon, J.; Bluestein, B. Summary of the technology for the manufacture of higher alpha-sulfo fatty acid esters. *J. Am. Oil Chem. Soc.* **1978**, *55*, 549–557. [CrossRef]

6. Ortega, J.A.T.; Medina, G.M.; Palacios, O.Y.S.; Castellanos, F.J.S. Mathematical Model of a Falling film Reactor for Methyl Ester Sulfonation. *Chem. Prod. Process Modeling* **2009**, *4*. [CrossRef]

7. Roberts, D.; Giusti, L.; Forcella, A. Chemistry of methyl ester sulfonates. *Biorenewable Resour.* **2008**, *5*, 2–19.

8. Afida, S.; Razmah, G.; Zulina, A. Biodegradation of Various Homologues of Palm-based Methyl Ester Sulphonates (MES). *Sains Malays.* **2016**, *45*, 949–954.

9. Kang, Y.; Ahmad Zahariah, I. Palm-based surfactants synergy in soap applications. In Proceedings of the 2001 PIPOC International Palm Oil Congress (Oleochemicals), Kuala Lumpur, Malaysia, 20–23 August 2001.

10. Pletnev, M. Vegetable-Derived Surfactants as a Reply to the Natural Trend in the Household and Personal Care. *SOFW J.* **2004**, *130*, 34–43.

11. Zolkarnain, N.; Maurad, Z.A.; Razmah, G.; Hazimah, A. Environmental Performance of Palm-Based Methyl Ester Sulphonates Production Using Life Cycle Approach. *J. Oil Palm Res.* **2016**, *28*, 104–113. [CrossRef]

12. Maurad, Z.A.; Ghazali, R.; Siwayanan, P.; Ismail, Z.; Ahmad, S. Alpha-sulfonated methyl ester as an active ingredient in palm-based powder detergents. *J. Surfactants Deterg.* **2006**, *9*, 161–167. [CrossRef]

13. *Fatty Methyl Ester Sulfonate (FMES) Market Analysis By End-Use (Personal Care, Detergents), By Region (North America, Europe, Asia Pacific, Central & South America, Middle East & Africa), Competitive Landscape, And Segment Forecasts, 2018–2025*; Grand View Research: San Francisco, CA, USA, 2017.

14. Yusof, N.Z.; Azizul Hasan, Z.A.; Abd Maurad, Z.; Idris, Z. Eye irritation potential: Palm-based methyl ester sulphonates. *Cutan. Ocul. Toxicol.* **2018**, *37*, 103–111. [CrossRef]

15. Dreger, E.; Klein, G.; Miles, G.; Shedlovsky, L.; Ross, J. Sodium Alcohol Sulfates. Properties Involving Surface Activity. *Ind. Eng. Chem.* **1944**, *36*, 610–617. [CrossRef]

16. Lim, W.H.; Ramle, R.A. The Behavior of Methyl Esters Sulphonate at the Water–Oil Interface: Straight-Chained Methyl Ester from Lauryl to Stearyl as an Oil Phase. *J. Dispers. Sci. Technol.* **2009**, *30*, 131–136. [CrossRef]

17. MacArthur, B.W.; Brooks, B.; Sheats, W.B.; Foster, N.C. Meeting the challenge of methylester sulfonation. In Proceedings of the 1999 PORIM International Palm Oil Congress: Emerging technologies and Opportunities in the Next Millennium, Kuala Lumpur, Malaysia, 1–6 February 1999; pp. 229–250.

18. Demirbaş, A. Bioethanol from cellulosic materials: A renewable motor fuel from biomass. *Energy Sources* **2005**, *27*, 327–337. [CrossRef]

19. Li, L.; Zhu, Y.-C. Research and application progress of fatty acid methyl ester sulfonates. *Deterg. Cosmet. J.* **2012**, *4*.

20. Hongping, H.; Ray, F.L.; Jianxi, Z. Infrared study of HDTMA+ intercalated montmorillonite. *Spectrochimica Acta Part A Mol. Biomol. Spectrosc.* **2020**, *60*, 2853–2859. [CrossRef]

21. Silverstein, R.M.; Bassler, G.C. Spectrometric identification of organic compounds. *J. Chem. Educ.* **1962**, *39*, 546. [CrossRef]

22. Elraies, K.A.; Tan, I.; Awang, M.; Saaid, I. The synthesis and performance of sodium methyl ester sulfonate for enhanced oil recovery. *Pet. Sci. Technol.* **2010**, *28*, 1799–1806. [CrossRef]

23. Jin, Y.; Tian, S.; Guo, J.; Ren, X.; Li, X.; Gao, S. Synthesis, characterization and exploratory application of anionic surfactant fatty acid methyl ester sulfonate from waste cooking oil. *J. Surfactants Deterg.* **2016**, *19*, 467–475. [CrossRef]

24. Babu, K.; Maurya, N.; Mandal, A.; Saxena, V. Synthesis and characterization of sodium methyl ester sulfonate for chemically-enhanced oil recovery. *Braz. J. Chem. Eng.* **2015**, *32*, 795–803. [CrossRef]

25. Kramer, H.; van Rosmalen, G. *Crystallization*; Academic Press: Amsterdam, The Netherlands, 2000.

26. Brunsteiner, M.; Jones, A.G.; Pratola, F.; Price, S.L.; Simons, S.J. Toward a molecular understanding of crystal agglomeration. *Cryst. Growth Des.* **2005**, *5*, 3–16. [CrossRef]

27. Guo, A.; Beddow, J.; Vetter, A. A simple relationship between particle shape effects and density, flow rate and Hausner ratio. *Powder Technol.* **1985**, *43*, 279–284. [CrossRef]

28. Larsson, K. Classification of glyceride crystal forms. *Acta Chem. Scand.* **1966**, *20*, 2255–2260. [CrossRef]

29. Lida, H.; Ali, A.R.M. Physico-chemical characteristics of palm-based oil blends for the production of reduced fat spreads. *J. Am. Oil Chem. Soc.* **1998**, *75*, 1625–1631. [CrossRef]

30. Marangoni, A.G. *Structure-Function Analysis of Edible Fats*; AOCS Press: Urbana, IL, USA, 2018.

31. AOCS Cj 2–95. *X-Ray Diffraction Analysis of Fats. Sampling and Analysis of Commercial Fats and Oils*; AOCS: Chicago, IL, USA, 1997.

32. Watanabe, H.; Morigaki, A.; Kaneko, Y.; Tobori, N.; Aramaki, K. Effects of temperature and humidity history on brittleness of α-sulfonated fatty acid methyl ester salt crystals. *J. Oleo Sci.* **2016**, *65*, 143–150. [CrossRef]

33. Segal, L.; Creely, J.; Martin, A., Jr.; Conrad, C. An empirical method for estimating the degree of crystallinity of native cellulose using the X-ray diffractometer. *Text. Res. J.* **1959**, *29*, 786–794. [CrossRef]

34. Xu, H.; Li, P.; Ma, K.; Welbourn, R.J.; Penfold, J.; Roberts, D.W. Adsorption of methyl ester sulfonate at the air–water interface: Can limitations in the application of the Gibbs equation be overcome by computer purification? *Langmuir* **2017**, *33*, 9944–9953. [CrossRef] [PubMed]

35. Stirton, A.; Wei, J.; Bistline, R. Sodium salts of alkyl α-sulfopalmitates and stearates. *J. Am. Chem. Soc.* **1953**, *75*, 4659–4960.

36. Weil, J.; Bistline, R.; Stirton, A. *Sodium Salts of Alkyl Alpha-Sulfopalmitates and Stearates*; Amer Chemical Soc 1155 16TH ST, NW 20036; Amer Chemical Soc: Washington, DC, USA, 1953; pp. 4859–4860.

37. Battaglini, G.T.; Larsen-Zobus, J.L.; Baker, T.G. Analytical methods for alpha sulfo methyl tallowate. *J. Am. Oil Chem. Soc.* **1986**, *63*, 1073–1077. [CrossRef]

38. Sheat, W. *Chemithon Analytical Methods*; The Chemithon Corporation: Seattle, WA, USA, 1994.

39. ASTM D. *3049 Standard Test Method for Synthetic Anionic Ingredient by Cationic Titration*; American Society for Testing and Materials: West Conshohocken, PA, USA, 1989.

40. Scholz, E. *Karl Fischer Titration: Determination of Water*; Springer: Berlin/Heidelberg, Germany, 2012.

41. Nikolic, A. *Fourier Transform Infrared Spectroscopy (FTIR)*; Kvalitet voda; Departman za hemiju, Prirodno-matematički fakultet Novi Sad: Novi Sad, Serbia, 2007.

42. Carr, R.L. Evaluating flow properties of solids. *Chem Eng.* **1965**, *18*, 163–168.

43. Hausner, H.H. *Friction Conditions in a Mass of Metal Powder*; Polytechnic Inst. of Brooklyn. Univ. of California: Los Angeles, CA, USA, 1967.